

# NMR probe for dynamic-angle spinning

K. T. Mueller, G. C. Chingas, and A. Pines

*Materials Sciences Division, Lawrence Berkeley Laboratory and Department of Chemistry, University of California, Berkeley, California 94720*

(Received 11 January 1991; accepted for publication 28 January 1991)

We describe the design of a probe for dynamic-angle spinning (DAS) NMR experiments, comprised of a spinning cylindrical sample holder whose axis may be reoriented rapidly between discrete directions within the bore of a superconducting magnet. This allows the refocusing of nuclear spin magnetization that evolves under anisotropic interactions such as chemical shift anisotropy and quadrupolar coupling, providing high resolution NMR spectra for quadrupolar nuclei in solid materials. The probe includes an axial air delivery system to bearing and drive jets which support and spin a rotor containing the sample. Axis reorientation is accomplished with a pulley attached to the probehead and coupled to a stepping motor outside of the magnet. The choice of motor and gear ratio is based on an analysis of the moments of inertia of the motor and load, the desired angular resolution, and simplicity of design. Control of angular accuracy and precision are discussed, as well as the efficiency of radiofrequency irradiation and detection. High resolution DAS spectra of oxygen-17 and aluminum-27 nuclei in polycrystalline minerals illustrate the experimental capabilities.

## I. INTRODUCTION

When a solid sample is placed inside a container that rotates rapidly about an axis inclined at an angle  $\theta$  with respect to a large magnetic field, the NMR spectral width due to the chemical shift interaction acquires a spatial dependence proportional to the second Legendre polynomial

$$P_2(\cos \theta) = \frac{1}{2}(3 \cos^2 \theta - 1). \quad (1)$$

It is possible to average away such first-order broadening by setting  $\theta$  to the magic angle of  $54.74^\circ$ , a zero of  $P_2(\cos \theta)$ .<sup>1,2</sup> The wide use of high resolution magic-angle spinning (MAS) to study spin- $\frac{1}{2}$  nuclei is testimony to the efficiency of this method for extracting the isotropic value of the chemical shifts for distinct nuclear environments in solid samples.<sup>3-5</sup>

Higher nuclear spin (quadrupolar) nuclei have non-spherical nuclear electric charge distributions that generally couple to local electric field gradients. For half-odd integer quadrupolar nuclei, which account for more than half of the NMR active isotopes in the periodic table, the effects of the quadrupolar coupling on the central ( $\frac{1}{2} \leftrightarrow -\frac{1}{2}$ ) transition enter only in second order.<sup>6-10</sup> The resulting lines are relatively narrow and may appear with enough sensitivity to provide structural information based on quadrupolar and chemical shift effects otherwise obscured by the much greater first-order broadening.

As with the chemical shift, second-order quadrupolar shifts have both an isotropic and anisotropic component. The total isotropic (orientation independent) NMR frequency depends on the trace of the chemical shift tensor, the quadrupolar coupling constant (strength of the electric field gradient), and the asymmetry of the electric field gradient. The anisotropic components depend on the orientation of the crystallite within the sample and tend to mask high-resolution structural information. In this case, spinning a powder sample narrows the lines only partially.<sup>11-15</sup> Examples of this phenomenon are found throughout the literature in spectra of quadrupolar nuclei such as oxygen-17 and alumi-

num-27 occurring in important materials such as minerals<sup>16,17</sup> and catalytic systems.<sup>18,19</sup>

It has recently become possible to remove both the first- and second-order anisotropic broadening in the NMR spectra of quadrupolar nuclei by two sample reorientation techniques: double rotation (DOR), where a sample spins in a small rotor embedded within a larger rotor,<sup>20-22</sup> and dynamic-angle spinning (DAS), where the axis of the spinning sample is moved in a plane between several discrete orientations.<sup>23,24</sup> Descriptions of devices that accomplish the double rotation motion have been published elsewhere.<sup>21,22</sup> Devices that flip the axis of a rotor have also been described, both for DAS<sup>24</sup> and for experiments providing two-dimensional correlations in solid-state NMR;<sup>25,26</sup> here we introduce a new dynamic-angle spinning apparatus.

Dynamic-angle spinning is similar to a conventional MAS experiment, but the spinning angle with respect to the laboratory reference frame (or magnet reference frame) is dynamic, as illustrated in Fig. 1 for the simplest case of two discrete orientations of the rotor axis. As with MAS of spin- $\frac{1}{2}$  nuclei, rapid spinning of a sample containing quadrupolar spins affects the anisotropic frequency shifts, but now a sum of two terms appears. One term is proportional to the second

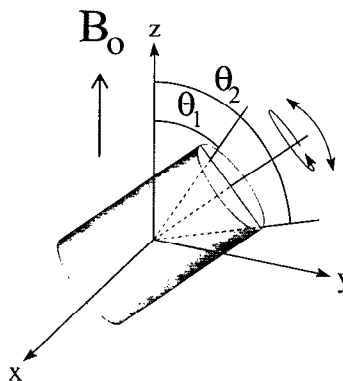


FIG. 1. The simplest case of dynamic-angle spinning: hopping of a rotor axis between two discrete orientations (defined by the angles  $\theta_1$  and  $\theta_2$ ) with respect to a large external magnetic field ( $B_0$ ) along the  $z$  axis.

Legendre polynomial of Eq. (1) above and the second is proportional to the fourth Legendre polynomial

$$P_4(\cos \theta) = \frac{1}{8}(35 \cos^4 \theta - 30 \cos^2 \theta + 3). \quad (2)$$

Clearly, single-axis spinning is incapable of simultaneous removal of broadening due to both terms, so spinning must be performed at a minimum of two angles for narrowing of resonances.

In a DAS experiment (with the central transition viewed as an isolated spin- $\frac{1}{2}$  manifold) the spin magnetization in each crystallite in a sample evolves first at an angle  $\theta_1$  for a time  $\tau_1$ , and then for a time  $\tau_2$  at a second angle  $\theta_2$ . When the angles and times are chosen so that the pair of conditions

$$\tau_1 P_2(\cos \theta_1) = -\tau_2 P_2(\cos \theta_2), \quad (3)$$

$$\tau_1 P_4(\cos \theta_1) = -\tau_2 P_4(\cos \theta_2) \quad (4)$$

are satisfied, evolution during  $\tau_2$  associated with both the second and fourth Legendre polynomials will cancel evolution during  $\tau_1$ . In this way, refocusing of all quadrupolar and chemical shift broadening is achieved. Evolution of the magnetization as a function of the total time  $t_1 = \tau_1 + \tau_2$  occurs only at isotropic frequencies, leading to narrowed resonance lines. We commonly choose  $\tau_1 = \tau_2$ , for which case Eqs. (3) and (4) have a solution corresponding to the symmetry of an icosahedron,<sup>27</sup>  $\theta_1 = 37.38^\circ$  and  $\theta_2 = 79.19^\circ$ . Further experimental details, such as the necessary pulse sequence of radio-frequency irradiation and the proper phase cycling of the detection are discussed in Ref. 24.

A mechanical device is required to rapidly reorient a spinning sample axis from  $\theta_1$  to  $\theta_2$ , synchronized with radio-frequency pulses to manipulate the nuclear spin magnetization. The need for quick reorientation of the axis is dictated by the relaxation of magnetization to thermal equilibrium (spin-lattice relaxation) and dipolar relaxation of spins in the energy levels of the central transition to other magnetic energy levels (cross relaxation and spectral diffusion). Angular accuracy is also necessary to sufficiently cancel the anisotropic evolution at the two angles, while reproducibility of the angles is essential due to the use of signal averaging and the two-dimensional nature of these experiments. We describe our design for an NMR probe to accomplish these ends and provide experimental demonstrations of the DAS technique.

## II. APPARATUS

Our aims for probe performance were short reorientation time, accurate and precise angular control, and radio-frequency efficiency, in that order. The following analysis led to this particular design. Assume that the motor used to drive the body through a hop has an essentially constant torque  $N_M$  over the required speed range. Neglecting friction, the power delivered by the motor during reorientation generates or absorbs rotational kinetic energy according to

$$\begin{aligned} N_M \omega_M &= \frac{d}{dt} \left( \frac{1}{2} I_M \omega_M^2 + \frac{1}{2} I_B \omega_B^2 \right) \\ &= I_M \omega_M \alpha_M + I_B \omega_B \alpha_B, \end{aligned} \quad (5)$$

where  $\omega_{M,B}$  and  $\alpha_{M,B}$  are the magnitudes of the angular velocities and accelerations of the motor ( $M$ ) and the body ( $B$ ) housing the rotor. We also assume that a transmission links the motor and body angles  $\theta_{M,B}$  by a ratio

$$\beta = \frac{\theta_B}{\theta_M} = \frac{\omega_B}{\omega_M} = \frac{\alpha_B}{\alpha_M}, \quad (6)$$

and that the inertia of the linkage is either incorporated or negligible. By eliminating the motor variables in Eq. (5) using Eq. (6) we arrive at the body acceleration:

$$\alpha_B = \frac{\beta N_M}{(I_M + \beta^2 I_B)}. \quad (7)$$

As a function of  $\beta$  this expression has a maximum value

$$\alpha_{\max} = \frac{N_M}{2\sqrt{I_M I_B}} = \frac{\alpha_0 \beta_0}{2}, \quad (8)$$

where  $\alpha_0 = N_M/I_M$  is the free-motor acceleration and  $\beta_0$  is the optimum transmission coupling factor,  $\sqrt{I_M/I_B}$ . This demonstrates that a massive motor having a large free acceleration will provide optimal speed performance, although, as we now show, this optimum is very insensitive to changes in mechanical parameters.

The parameter of direct interest is the reorientation time  $\tau_r$  required to move the rotor through an angle  $\Delta\theta = \theta_2 - \theta_1$  as above. Assuming ideal control, where the motor can be operated at any acceleration consistent with its torque, we may accelerate the rotor during the first half of the motion and decelerate it during the second half, so

$$\frac{\Delta\theta}{2} = \frac{1}{2} \alpha_B \left( \frac{\tau_r}{2} \right)^2, \quad (9)$$

and

$$\tau_r = 2 \sqrt{\frac{\Delta\theta}{\alpha_B}}. \quad (10)$$

We combine this with Eqs. (7) and (8) to obtain

$$\tau_r = \tau_{\min} \sqrt{\cosh \left[ \ln \left( \frac{\beta}{\beta_0} \right) \right]}, \quad (11)$$

where

$$\tau_{\min} = 2\sqrt{\Delta\theta/\alpha_{\max}}. \quad (12)$$

The appearance of hyperbolic functions is characteristic of impedance matching problems, of which this is a mechanical example.

The result in Eq. (11) shows a weak dependence of the reorientation time on almost all mechanical parameters, and the consequent difficulty of making substantial time reductions by mechanical improvements. The strongest dependences are upon the hop angle and motor torque/acceleration: these enter under square roots, and are the first parameters to optimize. We note that  $\tau_{\min}$  depends upon the fourth root of the moments of inertia. The square root expression in Eq. (11), which we call the time inflation factor, has a very weak dependence upon the optimal coupling condition, as the plot in Fig. 2 indicates. This is beneficial in the sense that it leaves the choice of the coupling parameter  $\beta$  relatively free.

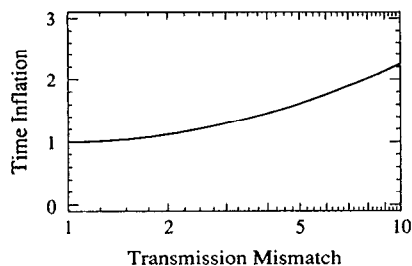


FIG. 2. Inflation factor of axis hopping time as a function of the transmission mismatch ( $\beta/\beta_0$ ).

We estimate what current technology offers. Fast motors have free accelerations in the range of  $10^5$ – $10^6$  rad/s<sup>2</sup>; moments of inertia span the range from  $10^{-5}$  to  $10^{-6}$  kg m<sup>2</sup>; the stator assemblies built to hold the rotor in our experiments have inertias that fall at the low end of this range. Given these ranges, and that  $\Delta\theta \approx \pi/4$ , we find that  $\tau_{\text{min}}$  spans the relatively narrow range from 1 to 4 ms, despite a variation of two orders of magnitude in the independent parameters. As we see below, however, such short times have not been achieved: the primary limiting factor is obtaining sufficiently subtle motion control for the motor performance to approach these theoretical limits.

Our motor selection was based largely on intrinsic acceleration. Because performance is such a weak function of  $\beta$ , while motor and body inertias are comparable, we chose direct drive ( $\beta = 1$ ) for control convenience. Although we considered a variety of gear and belt options, a simple string/pulley linkage seemed to be the lightest and simplest. We have used PMI (model USS-52M-006) and Sigma (model 803-D2220-F04) motors; Portescap P-series motors are also suitable for this type of design. All motors have comparable free accelerations, but the Sigma motors are preferable because of their larger torque and inertia.

We currently use a Whedco model IMC-1151-1-A controller to drive the motors. The IMC accepts commands and allows preprogramming of movement profiles using a PC as a dummy terminal. There are also external profile enable and trigger lines available which allow TTL level signals to trigger execution of profiles and commands within individual profiles. Movement commands, acceleration and deceleration rates, maximum speed, and start/stop pulse rates are loaded before an experiment is begun, and final control of the motor is through TTL level pulses sent to the IMC from the NMR spectrometer pulse programmer. Synchronization of movement with the radio-frequency pulses in the experiment is then easily accomplished with the spectrometer software. The basic laboratory setup for a DAS experiment is sketched in Fig. 3.

A schematic of the DAS probehead is shown in Fig. 4. The stator body and endcaps are shown placed on an aluminum platform, and the radio-frequency coil and  $\frac{1}{8}$ -in. diameter copper tubes for air delivery to the endcaps are also visible in this view. The coil is wound from copper magnet wire, but here it is shown as transparent to enhance the view of otherwise obscured components of the probehead. The assembly is built to fit within the 70 mm room temperature shims of a widebore superconducting magnet. The stator

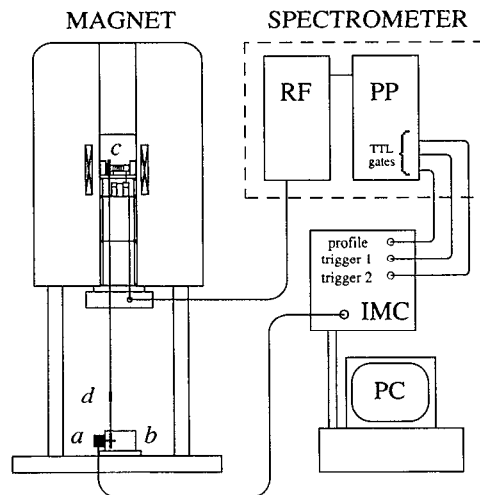


FIG. 3. Overview of the DAS experimental apparatus. The computer (PC) is used as a terminal to communicate with the intelligent motor controller (IMC). The IMC is controlled during the experiment with TTL-level signals from the NMR spectrometer pulse programmer (PP), which also controls the radiofrequency (RF) irradiation of the sample. The motor (*a*) is seated in the motor housing (*b*) at the base of the superconducting magnet. The motor action is coupled to the pulley seated on the probehead (*c*) with a string tightened using nylon turnbuckles (*d*) and fastened to a pulley on the motor shaft.

body and its internal parts (the stator sleeve and the rotor, discussed below) are machined from Vespel, a polyimide chosen for its high strength and ease of machinability. The endcaps and pulley are made of Delrin (polyacetal), a commercially available, less costly, high modulus plastic.

The cylindrical stator body (diameter 15.9 mm) is located by glass ball bearings (Microminiature Bearings Co.) in polyacetal races held in place by the endcaps. The bearings allow smooth, low friction reorientation. High pressure air is delivered through the endcaps and bearings to channels in the stator body.<sup>28</sup> This axial flow of air is undisturbed by the hopping motion, and no external hoses are needed which would add excess inertia to the assembly. A lightweight polycarbonate sleeve is positioned around the center of the

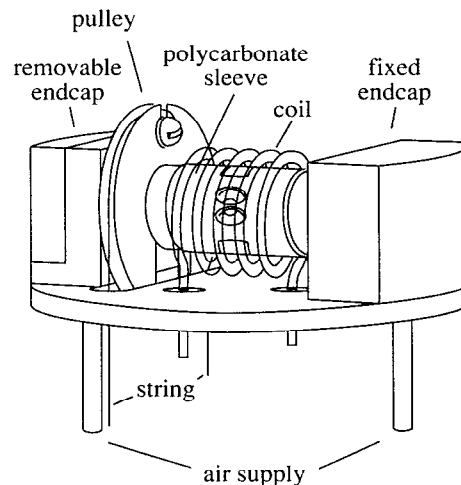


FIG. 4. Probehead for dynamic-angle spinning experiments.

stator body to keep the rotor in place.

Since a stationary rf coil surrounds the assembly, the stator body must be removed in order to change the sample. Removal of the pulley and unfastening of the side of one endcap (two screws) allows the stator body to slide out of the assembly, keeping one bearing set pressed around the end of the stator body while leaving the second pressed inside the fixed endcap. The former bearing outer race diameter is of slightly greater diameter than the stator body to allow removal.

The stator sleeve and sample holder are shown in the expanded drawing of Fig. 5. The sleeve is machined separately, press fitted into the stator body, and the whole assembly is turned on a lathe to preserve the cylindrical symmetry of the stator body. From one end of the stator body a single air hole feeds the center drive channel. The two outer bearing channels are also filled with pressurized air by splitting the axial channel from the other endcap into two channels which meet the stator cavity near the circumference of the stator body. Air forced through the 12 radial bearing holes (0.3 mm diameter) at each end of the stator supports the rotor. Each circle of bearing holes are at a 45° angle with respect to the cylindrical axis of the stator sleeve to keep their exit ports as near the ends of the rotor as possible. This maximizes support, allowing use of the longest (and therefore most stable) rotors. The bearing air escapes through the top and bottom of the rotor chamber.

We found that approximately 30 psi of bearing pressure was required to prevent rotor touchdown during hops. The effect of a hop on a rapidly spinning rotor is discussed in Appendix A. The conclusion is that crashes associated with hops are due to dynamic disturbances that disrupt ordinarily stable equilibrium air patterns, and not failure of the bearings to support the excess load caused by the moving rotor. The six drive holes (1.0 mm diameter) are in the plane orthogonal to the spinning axis and are directed tangentially to give the air a rotary flow component when impinging upon the wide rotor flutes. The air provides torque to the rotor, moving up and down the flutes to then be released quickly to

the laboratory through the escape holes. The escape holes are also drilled tangentially, but in a direction opposite to that of the drive holes and offset by one-sixth of the distance around the circumference of the stator. This presumes an impulse rather than reaction drive, which is consistent with improved performance obtained by lengthening the rotor flutes. We decoupled the two air delivery and escape paths in this way to minimize the turbulent flow of air within the vicinity of the rotor, with the intent of increasing spinning stability and reliability. Drive pressures of 60 to 70 psi are necessary to provide routine rotor spinning frequencies of 5 to 6 kHz using 6.3-mm-diam rotors.

The rotors themselves are 15.9 mm long with conical screw caps on either end. Twelve flutes are centered along the body, having a length of 4.0 mm and a depth of 0.3 mm. The total sample volume is 0.15 cm<sup>3</sup> in a standard rotor with 1.0 mm wall thickness. Flat spacers within the rotors separate the powdered sample material from an angular standard (usually potassium bromide or deuterated 1,4-dimethoxybenzene) used to set the magic angle. The rotor is held in place longitudinally with a thin polycarbonate sleeve rather than more conventional fixed endcaps to optimize the rotor length while minimizing both the coil volume and stator body moment of inertia. Holes are cut in the ends and the sides of this sleeve to allow free discharge of the bearing and drive air. The conical ends of the rotors slowly wear away at the bearing points on the sleeve and this piece typically needs replacement after 500 h of operation.

The pulley has a diameter at the bottom of the string guide of 31.8 mm. It slides onto a square slot on the stator body, and has a notch cut into one side of the string guide for passage of the string to a fastening screw. The string is a length of Kevlar (Dupont aramid fiber) with a diameter of approximately 0.8 mm. At the base of the magnet, the string is also attached to a second pulley mounted on the shaft of the stepping motor. A similar notch and fastening screw are present on the lower pulley, providing an efficient coupling of angular position with negligible mechanical backlash. The string is tightened with turnbuckles between the bottom pulley and the base of the magnet shim stack (see Fig. 3).

An external, fixed-coil arrangement is used for irradiation with the radio-frequency ( $B_1$ ) field. This sacrifices electrical efficiency, but surmounts problems experienced with an earlier moving coil design.<sup>24</sup> Specifically, tuning changes associated with axis motion and difficulty with sliding contacts or moving leads are avoided. A major advantage of this arrangement is equivalent performance at all angles: pulse lengths for 90° nutation of the magnetization are independent of the axis orientation, and it is possible to perform NMR experiments at any axis angle, including 0°. This latter axis orientation results in a signal which is equivalent to that obtained from a static sample, and allows two-dimensional NMR spectroscopy correlating the powder pattern line-shapes observed from a static sample with the high resolution lines provided by DAS (or MAS) narrowing.

### III. PERFORMANCE AND EXPERIMENTAL RESULTS

To investigate the performance of the probe, the strong time-domain free induction decay (FID) signal is observed

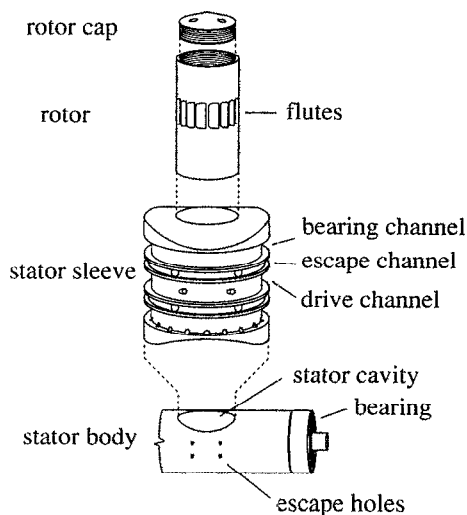


FIG. 5. Expanded view of the stator body, stator sleeve, and rotor. The stator body is shown reduced in size relative to the other components.

after a  $90^\circ$  pulse is applied to the deuterium nuclei in a rotating sample of deuterated 1,4-dimethoxybenzene. The deuterium nucleus (spin-1) is affected by first-order quadrupolar interactions, which are motionally averaged while spinning at the magic angle.<sup>11,29</sup> Since the distribution of resonance frequencies is large (on the order of 75 kHz at 9.4 T) the inhomogeneous static lineshape in the frequency domain is broken up into spinning sidebands, symmetrically displaced about a central (isotropic) peak and occurring at integer multiples of the rotor frequency. Away from the magic angle, the two degenerate  $\Delta m = 1$  transitions obtain different isotropic frequencies and the resonance splits into a doublet. When exactly at the magic angle the inverse Fourier transform of the isotropic signal and its envelope of sidebands, a time domain FID composed of a train of rotational echoes occurring once every rotor cycle, is observed. The sensitivity of the time and frequency domain signals to the angle of the spinning axis with respect to the external field is demonstrated in Fig. 6. Under typical experimental conditions, the step size used is obtained from one-sixteenth stepping of a 200 step per revolution motor, or  $0.1125^\circ/\text{step}$ . Moving through the magic angle in one step increments verifies the suitability of the magic-angle condition as a mark for determining absolute axis orientation.

The hop in a DAS experiment is made between  $\theta_1 = 37.38^\circ$  and  $\theta_2 = 79.19^\circ$ , a difference of  $41.81^\circ$ . The nearest angles obtainable with the magic angle of  $54.74^\circ$  as a fixed reference and  $0.1125^\circ$  angular resolution are  $\theta_1 = 37.41^\circ$  and  $\theta_2 = 79.15^\circ$ , a difference of  $41.74^\circ$  or 371 steps. When the spinning axis is set 371 steps off of the magic angle, the time necessary to complete a hop of  $41.74^\circ$  is determined by initiating the return hop to the magic angle and waiting a set delay time before applying a pulse to the system. The FID is then recorded, and the delay varied until an FID matching

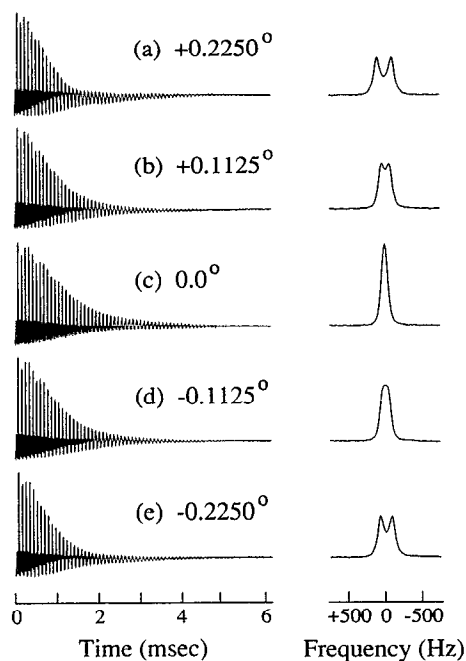


FIG. 6. Free induction decay (FID) signals and the resulting isotropic peaks from deuterium nuclei in deuterated 1,4-dimethoxybenzene as a function of angular offset of the rotor axis from the magic angle.

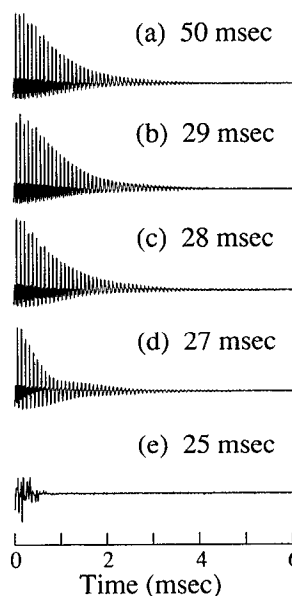


FIG. 7. Decays after hopping  $41.74^\circ$  with a variety of delay times, allowing determination of the hopping time necessary for the DAS experiment.

that of Fig. 6(c) is observed. The decays in Fig. 7 show the effect of changing the time allowed for the hop. We observe undistorted signals 28 ms after the initiation of an axis hop, corresponding to measured motor drive current pulses of 25 ms, and an inferred settling time of 3 ms. This is much less than the 100 msec or longer longitudinal relaxation times ( $T_1$ ) of many quadrupolar nuclei in solids, and is therefore sufficiently short to allow storage of the signal during the reorientation with negligible loss in signal intensity.

We attempted to increase the speed of the hop by increasing the acceleration of the motor through its triangular speed profile. This led to decreased performance because of angular overshoot. A smaller start/stop pulse rate was then necessary, leading to overall slower performance. The use of optical encoder feedback could not compensate completely for the overshoot as a finite time (on the order of a few ms) is required to search for the desired final angle.

The experimental results obtainable with this design are illustrated with two examples from the NMR spectroscopy of quadrupolar nuclei in solid minerals. The first example is from a sample of the pyroxene diopside ( $\text{CaMgSi}_2\text{O}_6$ ) which has been enriched to 20% in oxygen-17: this is the only magnetically active isotope of oxygen (spin- $\frac{5}{2}$ ). The MAS spectrum of the oxygen-17 in diopside, obtained in a 9.4 T magnetic field, is shown in Fig. 8(a). The three crystallographically distinct oxygen sites each contribute a broad resonance and it is impossible to fully resolve the distinct resonances at this field strength. Since the breadth of the patterns scale with the inverse of the magnetic field strength, it would be possible to resolve these resonances using a larger magnetic field. However, it has been calculated that a field in excess of 45 T would be necessary to provide sufficient narrowing.<sup>30</sup> The high-resolution DAS spectrum for the same compound at 9.4 T is in Fig. 8(b).<sup>31</sup> The spectrum was obtained by performing a one-dimensional DAS experiment over a period of 2.5 days (five averages of a full eight experiment phase cycle, 256 complex data points accumulated with a 20 s recycle delay). In the DAS spectrum, three narrow resonances (150 Hz linewidths) are observed corresponding to the three distinct oxygen environments in

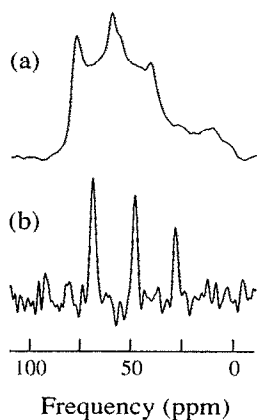


FIG. 8. (a) Magic-angle spinning (MAS) spectrum of oxygen-17 in diopside ( $\text{CaMgSi}_2\text{O}_6$ ) at a spectrometer frequency of 54.25 MHz (9.4 T). (b) One-dimensional DAS spectrum of diopside. A 256 point complex interferogram was acquired and Fourier transformed with 75 Hz (1.4 ppm) Lorentzian broadening. The frequency axis is referenced to oxygen-17 in water (37.5% enriched).

the unit cell.<sup>32</sup> The two higher frequency resonances are associated with the two terminal oxygens in the diopside structure, while the lower frequency resonance corresponds to the bridging oxygen with a larger quadrupolar coupling frequency. The role of the oxygen *p*-orbital occupancy, and its relation to bridging oxygens and their larger local electric field gradients, is discussed by Janes and Oldfield.<sup>33</sup>

Dynamic-angle spinning is intrinsically a two-dimensional NMR experiment, where the first dimension yields a high resolution spectrum with narrow lines observed at an isotropic frequency. The second dimension is the anisotropic powder pattern at the second spinning angle (usually 79.19°) associated with its isotropic shift in the first dimension. A method for obtaining pure absorption phase DAS lineshapes has been developed<sup>34</sup> which allows a second axis flip in the experiment. The advantages gained from this variation are narrower lineshapes in a two-dimensional display and correlation of the second dimension in the DAS experiment with anisotropic NMR spectra at *any* spinning angle. We choose the magic angle ( $\theta = 54.74^\circ$ ) as the final angle in order to average residual dipolar interactions and chemical shift anisotropy present at any other angle.

An example of two-dimensional pure absorption phase DAS is shown in Fig. 9 for the aluminum-27 resonance obtained at 9.4 T from the single aluminum site present in petalite ( $\text{LiAlSi}_4\text{O}_{10}$ ), a polycrystalline lithium ore. For this sample, a pair (real and imaginary data sets) of 512 experiments were performed at increasing values of  $t_1$ , accumulating 256 complex points in the second time dimension. The two-dimensional hypercomplex Fourier transformation shows a narrower line (approximately 5 ppm) in the high resolution DAS dimension, compared to the 54.74° anisotropic lineshape in the second frequency dimension. The single peak in the DAS spectrum appears at a total isotropic shift of 46 ppm with respect to aluminum-27 in a saturated  $\text{Al}(\text{NO}_3)_3$  solution. The second dimension corresponds to the MAS spectrum which may be simulated using a computer and a least-squares fitting program to refine the quadrupolar parameters. We find  $e^2qQ/h = 4.62 \pm 0.05$  MHz with an asymmetry parameter  $\eta$  of  $0.48 \pm 0.03$  and these results are in excellent agreement with those calculated from recent dc SQUID measurements on the same sample.<sup>35</sup> The isotropic chemical shift is then calculated to be 59 ppm with respect to the standard  $\text{Al}(\text{NO}_3)_3$  solution. This result bodes

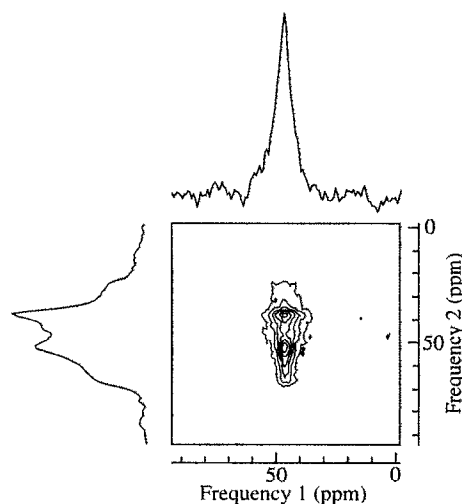


FIG. 9. Pure absorption two-dimensional DAS spectrum of aluminum-27 in petalite ( $\text{LiAlSi}_4\text{O}_{10}$ ) at a spectrometer frequency of 104.27 MHz (9.4 T). Two 512 by 256 complex data arrays were acquired and a two-dimensional hypercomplex Fourier transform was performed. Lorentzian broadening of 50 Hz (0.5 ppm) was applied in the first dimension, while 100 Hz (1 ppm) was applied in the second. Frequency axes are referenced to aluminum-27 in saturated aqueous  $\text{Al}(\text{NO}_3)_3$ .

well for the separation and complete determination of quadrupolar parameters from overlapping resonances like those in the diopside sample, using the DAS dimension to separate lineshapes in the powder (low resolution) dimension which may then be simulated individually.

#### IV. DISCUSSION

This discussion has provided an analysis and implementation of a dynamic-angle spinning probe suitable for narrowing resonance lines in spectra of quadrupolar nuclei. This design offers several advantages in its present form. Relatively simple mechanical construction has provided reliable operation and reasonable hopping times using commercially available mechanical drives. The stationary rf coil eliminates potential difficulties associated with moving rf circuit components and complications due to changing the irradiation direction, and permits use of all axis angles with equal efficiency. The observation frequency is also easy to change, often accomplished with a simple change of irradiation coil. Overall, this probe is well suited for homonuclear dynamic-angle correlation studies of nuclei with moderate sensitivity and reasonable relaxation rates. It is clear that there is room for improvement in several areas: we expect that attention to controller electronics could reduce hopping times below 10 ms, and that a more compact coil design could improve the filling factor and overall rf performance, as well as allowing higher frequency operation. It would likewise be useful to extend probe versatility by incorporating features such as heteronuclear decoupling and variable temperature capability.

#### ACKNOWLEDGMENTS

We thank J. Sachleben, T. Tammer, D. Colomb, and D. Murai for experimental assistance and probe construction;

B. Q. Sun, P. Grandinetti, and S. P. Rucker for helpful discussions; and J. Baltisberger for spectral simulations. Doctor J. Stebbins kindly provided the petalite and diopside samples. K. T. M. is an NSF Graduate Fellow. This work was supported by the Director, Office of Energy Research, Office of Basic Energy Sciences, Materials Science Division of the U.S. Department of Energy under Contract No. DE-AC03-76SF00098.

## APPENDIX A

We consider the torques arising from the reorientation of a rotor spinning at an angular velocity  $\omega$  and supported by air bearings a fixed distance  $B$  from the rotor center. The rotor with mass  $M$  has height  $H$  and radius  $R$ . We assume that the reorientation axis is along the  $x$ -axis such that the sample rotation axis is always in the  $yz$  plane: the angle  $\theta$  describes the angle which the spinning axis makes with the  $z$  direction.

If the angular velocity of the spinning axis reorientation is  $\Omega = d\theta/dt$  then the angular momentum  $\mathbf{L}$  at any instant is

$$\mathbf{L} = \omega I_0 (\hat{\mathbf{e}}_z \cos \theta + \hat{\mathbf{e}}_y \sin \theta) + \Omega I_1 \hat{\mathbf{e}}_x, \quad (\text{A1})$$

where  $I_0$  and  $I_1$  denote moments of inertia parallel and perpendicular to the cylindrical rotor axis respectively. Explicitly

$$I_0 = MR^2/2 \quad (\text{A2})$$

and

$$I_1 = \frac{MR^2}{4} \left( 1 + \frac{H^2}{3R^2} \right). \quad (\text{A3})$$

To obtain the torque, we differentiate Eq. (A1) with respect to time and obtain two additive terms:

$$\mathbf{N}_g = \omega \Omega I_0 (-\hat{\mathbf{e}}_z \sin \theta + \hat{\mathbf{e}}_y \cos \theta) \quad (\text{A4})$$

and

$$\mathbf{N}_r = \alpha I_1 \hat{\mathbf{e}}_x, \quad (\text{A5})$$

where  $\alpha = d\Omega/dt$  is the angular acceleration of the reorientation. Note that the torque  $\mathbf{N}_r$  is identical to that generated by reorienting a nonspinning cylinder. The gyroscopic torque,  $\mathbf{N}_g$ , arises from the fact that a spinning object is being realigned: it depends on the product of the two angular velocities,  $\omega$  and  $\Omega$ . Since  $\mathbf{N}_g$  is at all times orthogonal to the drive axis it will be borne completely by the bearings that hold the stator and the motor need only provide a torque equal to  $\mathbf{N}_r$  to effect the motion. This leads to the first important conclusion: a spinning sample is no more difficult for the motor to reorient than one that is static. Of course, the *air* bearings between the stator sleeve and the rotor must provide forces to support both of these torques. Empirically, this bearing load may be significant, since rotor touchdown associated with reorientation is observed unless bearing pressures of 30 psi are maintained.

Consider the case where reorientation through an angle  $\Delta\theta$  occurs in a time  $\tau_r$  and consists of a uniform angular acceleration ( $\alpha$ ) from rest up to a maximum angular velocity ( $\Omega_{\max}$ ) during the first half of the reorientation. Uniform deceleration back to rest results in an overall triangular velocity profile and Eq. (A4) shows that the peak gyroscopic

torque occurs at the midpoint of the motion where the angular velocity is

$$\Omega_{\max} = \alpha \tau_r / 2. \quad (\text{A6})$$

Using Eq. (9) in the main text we may relate  $\Omega_{\max}$  to  $\Delta\theta$  and  $\tau_r$ , finding

$$\Omega_{\max} = 2\Delta\theta / \tau_r. \quad (\text{A7})$$

Equation (A5) indicates that the reorientation torque is constant during the acceleration and simply undergoes a sign change when the motion changes to deceleration. The ratio of the torques may then be calculated:

$$\frac{|\mathbf{N}_r|}{|\mathbf{N}_g(\max)|} = \frac{\alpha}{2\omega\Omega_{\max}} \times \left( 1 + \frac{H^2}{3R^2} \right) = \frac{[1 + (H^2/3R^2)]}{\omega\tau_r}. \quad (\text{A8})$$

For typical cylinder aspect ratios ( $H/2R$ ) between 2 and 5, the numerator of Eq. (A8) falls between 1 and 35. The denominator, on the other hand, is the number of radians the rotor turns while it is undergoing reorientation. For a 5 kHz spinning rate and reorientation times between 10 and 50 msec, this falls between 300 and 1500. The second important conclusion then is that the main air bearing load associated with reorientation is generated by gyroscopic reaction forces.

To estimate the magnitude of the load associated with hopping in more familiar terms, we will calculate how large a sample packing imbalance is required to generate a bearing load comparable to that expected during reorientation. We characterize rotor imbalance by the parameter  $\eta = \Delta R/R$ , where  $\Delta R$  is the distance of the actual center of gravity from the spinning axis and  $R$  is again the rotor radius. For a symmetric imbalance, the force on each of a pair of bearings holding the rotor is

$$F_b = \eta \omega L / R, \quad (\text{A9})$$

where  $\omega$  and  $L$  are the magnitudes of the rotor angular velocity and momenta as defined above.

On the other hand, if we move the spinner with an angular velocity of reorientation  $\Omega$  about an axis perpendicular to the spinning axis, we require a peak force per bearing

$$F_r = \Omega_{\max} L / 2B, \quad (\text{A10})$$

where  $B$  is the offset of bearing ring from the spinner center.

To obtain the equivalent imbalance  $\eta_{\text{eq}}$  required to generate a force equal to the reorientation load, we equate Eqs. (A9) and (A10), obtaining

$$\eta_{\text{eq}} = \left( \frac{R}{2B} \right) \left( \frac{\Omega_{\max}}{\omega} \right). \quad (\text{A11})$$

To a first approximation,  $R/B = 1$ ,  $\Omega_{\max} = \pi/(2\tau_r)$ , and  $\omega = 2\pi/\tau_s$ , where  $\tau_r$  and  $\tau_s$  are the reorientation time and spinning period, respectively. This leads to  $\eta_{\text{eq}} = \tau_s/8\tau_r$ . For  $\tau_s = 0.2$  ms and  $\tau_r = 30$  ms, we find the equivalent offset to be one part in 1200. This is a very small value and it is not expected to affect spinner stability during the hop.

This analysis has shown that the magnitudes of the reorientation torques are smaller or comparable to those occurring in steady state motion. However, bearing failure is ob-

served during reorientation if bearing pressures are too low. Such failure may then be due to more complex motions, possibly involving gyroscopic oscillations and air bearing compression. Whatever the mechanism for the bearing failure, it is still possible to perform the necessary rapid reorientation of a spinning rotor to accomplish the DAS experiments as sufficient bearing pressures are easily maintained with this design.

- <sup>1</sup>I. J. Lowe, *Phys. Rev. Lett.* **2**, 285 (1959).  
<sup>2</sup>E. R. Andrew, A. Bradbury, and R. G. Eades, *Nature (London)* **183**, 1802 (1959).  
<sup>3</sup>C. A. Fyfe, *Solid State NMR for Chemists (CFC, Guelph, 1983)*.  
<sup>4</sup>G. E. Maciel, *Science* **226**, 282 (1984).  
<sup>5</sup>C. P. Slichter, *Principles of Magnetic Resonance*, 3rd ed. (Springer, New York, 1989), pp. 392–406.  
<sup>6</sup>R. V. Pound, *Phys. Rev.* **79**, 685 (1950).  
<sup>7</sup>M. H. Cohen and F. Reif, *Solid State Phys.* **5**, 321 (1957).  
<sup>8</sup>G. M. Volkoff, *Can. J. Phys.* **31**, 820 (1953).  
<sup>9</sup>P. A. Casabella, *J. Chem. Phys.* **40**, 149 (1964).  
<sup>10</sup>K. Narita, J. Umeda, and H. Kusumoto, *J. Chem. Phys.* **44**, 2719 (1966).  
<sup>11</sup>E. R. Andrew and R. G. Eades, *Disc. Faraday Soc.* **34**, 38 (1963).  
<sup>12</sup>E. Kundla, A. Samoson, and E. Lippmaa, *Chem. Phys. Lett.* **83**, 229 (1981).  
<sup>13</sup>H.-J. Behrens and B. Schnabel, *Physica* **114B**, 185 (1982).  
<sup>14</sup>A. Samoson, E. Kundla, and E. Lippmaa, *J. Magn. Reson.* **49**, 350 (1982).  
<sup>15</sup>S. Ganapathy, S. Schramm, and E. Oldfield, *J. Chem. Phys.* **77**, 4360 (1982).  
<sup>16</sup>R. J. Kirkpatrick, K. A. Smith, S. Schramm, G. Turner, and W.-H. Yang, *Ann. Rev. Earth Planet. Sci.* **13**, 29 (1985).  
<sup>17</sup>R. J. Kirkpatrick, in *Spectroscopic Methods in Mineralogy and Geology*, Mineralogical Society of America, Reviews in Mineralogy, edited by F. C. Hawthorne (Mineralogical Society of America, Washington, DC, 1988), Vol. 18, pp. 341–403 and references therein.  
<sup>18</sup>H. K. C. Timken, G. L. Turner, J.-P. Gilson, L. B. Welsh, and E. Oldfield, *J. Am. Chem. Soc.* **108**, 7231 (1986).  
<sup>19</sup>H. K. C. Timken, N. Janes, G. L. Turner, S. L. Lambert, L. B. Welsh, and E. Oldfield, *J. Am. Chem. Soc.* **108**, 7236 (1986).  
<sup>20</sup>A. Samoson, E. Lippmaa, and A. Pines, *Mol. Phys.* **65**, 1013 (1988).  
<sup>21</sup>A. Samoson and A. Pines, *Rev. Sci. Instrum.* **60**, 3239 (1989).  
<sup>22</sup>Y. Wu, B. Q. Sun, A. Pines, A. Samoson, and E. Lippmaa, *J. Magn. Reson.* **89**, 297 (1990).  
<sup>23</sup>A. Llor and J. Virlet, *Chem. Phys. Lett.* **152**, 248 (1988).  
<sup>24</sup>K. T. Mueller, B. Q. Sun, G. C. Chingas, J. W. Zwanziger, T. Terao, and A. Pines, *J. Magn. Reson.* **86**, 470 (1990).  
<sup>25</sup>A. Bax, N. M. Szeverenyi, and G. E. Maciel, *J. Magn. Reson.* **55**, 494 (1983).  
<sup>26</sup>T. Terao, H. Miura, and A. Saika, *J. Chem. Phys.* **85**, 3816 (1986).  
<sup>27</sup>A. Samoson, B. Q. Sun, and A. Pines, LBL Report No. 28400 (to be published).  
<sup>28</sup>This is similar to the design of the double rotor apparatus. See Refs. 21 and 22.  
<sup>29</sup>C. Ye, B. Sun, and G. E. Maciel, *J. Magn. Reson.* **70**, 241 (1986).  
<sup>30</sup>E. Oldfield (private communication). Also see B. F. Chmelka, K. T. Mueller, A. Pines, J. Stebbins, Y. Wu, and J. W. Zwanziger, *Nature (London)* **339**, 42 (1989).  
<sup>31</sup>K. T. Mueller, Y. Wu, B. F. Chmelka, J. Stebbins, and A. Pines, *J. Am. Chem. Soc.* **113**, 32 (1991).  
<sup>32</sup>B. Warren and W. L. Bragg, *Z. Kristallogr.* **69**, 168 (1928).  
<sup>33</sup>N. Janes and E. Oldfield, *J. Am. Chem. Soc.* **108**, 5743 (1986).  
<sup>34</sup>K. T. Mueller, E. W. Wooten, and A. Pines, *J. Magn. Reson.* (in press).  
<sup>35</sup>C. Conner, J. Chang, and A. Pines, *J. Chem. Phys.* **93**, 7639 (1990).